MOLEKUL
eISSN: 2503-0310

Articles
https://doi.org/10.20884/1.jm.2025.20.3.12428

Computational Study on Apoptosis-Inducing Factor (AIF)-Mediated Modulation of Menadione using Molecular Docking and Parametrized Quantum Methods

Muklisatum Listyawati[1,2], Suci Zulaikha Hildayani[3], Mia Ledyastuti[4], Fida Madayanti Warganegara[5], Muhamad Abdulkadir Martoprawiro[4]*

[1] Doctoral Program of Chemistry, Faculty of Mathematics and Natural Science, Institut Teknologi Bandung, Indonesia
[2] Faculty of Islamic Education, Institut Agama Islam Uluwiyah Mojokerto, Mojokerto 61382, Indonesia
[3] Research Center for Computing, National Research and Innovation Agency, Bandung, Indonesia
[4] Inorganic and Physical Chemistry Research Group Faculty of Mathematics and Natural Sciences, Institut Teknologi Bandung, Indonesia
[5] Biochemistry Research Group, Faculty of Mathematics and Natural Science, Institut Teknologi Bandung, Indonesia

*Corresponding author email: muhamad@itb.ac.id

Received June 25, 2024; **Accepted** September 27, 2025; **Available online** November 20, 2025

ABSTRACT. Apoptosis-inducing factor (AIF) is a protein that is crucial for apoptosis which its dysregulation has been connected to the emergence of cancer. Mitochondria are organelles that in healthy cells function as energy factories that are important for maintaining cell life. AIF is located in the mitochondrial intermembrane space with active sites, namely FAD and NADH. Meanwhile in the recent studies, quinone compounds have shown potential as anti-cancer agents by targeting mitochondrial function, but the mechanism is still unclear. In this study, we used computational methods, including molecular docking and the Divide-and-Conquer Density Functional Tight-Binding Molecular Dynamics (DCDFTBMD) method, a type of parametrized quantum calculation, to investigate the interaction between mitochondrial AIF and menadione, as a quinone compound with anticancer potential. From the calculation result, AIF interaction with menadione was stronger in the FAD domain than in NADH. The partial charges of the ligands before and after the interactions were calculated using the DCDFTBMD technique, and the results show that the charge in the bonding area becomes more negative. This indicates the strengthening of electrostatic interactions through polarization effects in the bonding molecule. Additionally, it was discovered through this study's data that all ligands interacted with the ser-175 residue in the AIF protein. These residues are modulated by the involvement of AIF in the cell death process. From this study, it can be concluded that menadione has the potential as an anticancer agent through the AIF modulation mechanism.

Keywords: AIF, enzyme-catalyzed modulation, docking, quantum parametrization, menadione

INTRODUCTION

Organelles called mitochondria carry out the processes of cell death and cell survival in healthy cells, respectively. These organelles function as energy factories in healthy cells, producing ATP molecules and the primary fuel for cell survival through the respiratory chain (Galuzzi et al., 2007; Kroemer et al., 2007). Apoptosis Inducing Factor (AIF) is a mitochondrial oxidoreductase protein involved in apoptosis and energy metabolism (Misevicience et al., 2011; Bano & Prehn, 2018). In healthy cells, AIF in mitochondria plays a crucial role in redox reactions and bioenergetics. AIF contains a C-terminal domain and binding domains, namely NAD and FAD. AIF domains can play a role in cell survival and death. Several studies have shown that both roles of AIF occur through redox processes (Bano & Prehn, 2018 & Galluzi et al., 2007).

Apoptosis is induced through extrinsic and intrinsic pathways based on trigger mechanisms (Lorenzo et al., 1999). The extrinsic pathway is activated by cell death factors, such as FAS and TNFR1, which ultimately activate caspase-8. The intrinsic pathway is regulated by a balance between proapoptotic and antiapoptotic proteins, and is triggered by the release of cytochrome-c from mitochondria and the activation of caspase-9 (Fang & Peng, 2022). Apoptosis is primarily caused by calcium influx, which activates caspases and calpains. Cell and oligodendrocyte death can be mediated by cytokines such as TNF-α, free radicals, and excitotoxicity. FAS-mediated cell death plays a role in oligodendrocyte apoptosis and inflammatory responses in the acute and subacute stages. A role that has been discovered for AIF is its activity in the metabolism of quinone compounds, such as menadione (2-methyl-1,4-naphthoquinone; vitamin

K3), by acting as NADH quinone reductase that facilitates the reduction reaction of quinone to toxic semiquinone or hydroquinone compounds (Galuzzi et al., 2007; Fang & Peng, 2022; Jha & Kumar, 2024). In addition, studying the role of mitochondrial AIF death is very important, especially with regard to the development of cells induced to die, through the permeability of the mitochondrial outer membrane (Hangen et al., 2020). AIF, which is initially located in the mitochondria, translocates to the cytoplasm and then to the nucleus to participate in chromatin condensation and DNA degradation. Meanwhile, menadione is a third family of cytotoxic quinones that reacts within cells through its reducing and arylation capacity (Wiraswati et al., 2016; Szeliga & Rola, 2022). This study aims to confirm the NADH domain of FAD domain in the cell death process and study its interaction with quinone compounds which have the potential as native ligands that play an important role in computational oncology.

In this study, we used a computational approach to investigate the interactions between mitochondrial AIF and a series of quinone compounds with known anticancer potential. Docking methods were used to predict the binding modes of the quinone compounds within the AIF active site. Docking simulations provided insights into the molecular recognition and binding affinity of these compounds, offering a preliminary assessment of their potential as AIF inhibitors (Vidal-Limon et al., 2022; Abad et al., 2013). In addition, to gain a more comprehensive understanding of the interactions of AIF-quinone compounds, we used the Density-Functional Tight-Binding Molecular Dynamics (DCDFTBMD) method. DCDFTBMD combines the accuracy of density functional theory (DFT) with the computational efficiency of tight-binding approximations, allowing us to simulate the dynamics of AIF-quinone complexes on realistic time scales (Nishimura & Nakai, 2019). By performing molecular dynamics simulations, we aimed to elucidate the stability, flexibility, and conformational changes of the AIF-quinone complex, providing valuable insights into the binding mechanism and the role of specific amino acid residues in the interaction. This information can guide the design and optimization of quinone-based compounds as potential anticancer agents targeting mitochondrial AIF (Acacio et al., 2022; Cores et al., 2023). The results of this computational study have the potential to contribute to the development of novel therapies that selectively modulate AIF function, leading to improved cancer treatment options. Furthermore, the computational approach presented here demonstrates the benefits of combining docking and dynamics simulations to investigate protein-ligand interactions, thereby complementing experimental studies and accelerating the drug discovery process. Overall, this study serves as a computational framework to explore the interaction between mitochondrial AIF and quinone compounds, revealing their potential as anticancer agents. The integration of docking methods and DCDFTBMD simulations provides valuable insights into the binding mechanism and dynamics of the AIF-quinone complex, facilitating the development of targeted therapies for cancer treatment (Nakai et al., 2016; Sevrioukova, 2009; Aditya et al., 2017).

EXPERIMENTAL SECTION

Computational Details

The calculation method uses Density Functional Theory (DFT) using B3LYP functional and def2-svp basis sets geometry optimization of ligands FAD, NADH, menadione, glutathione (GSH), and thiodione. Also used software Autodock Vina, NAMD and DCDFTBM that implemented in a Python environmental. Crystal structure of Apoptosis Inducing Factor (AIF) with Protein Data Bank (PDB) code 3GD4 (http://www.rscb.org/pdb). The 2 native ligands of each enzyme used are Flavin Adenine Dinucleotide (FAD) and Nicotinamide Adenine Dinucleotide (NADH). The ligands of quinone compounds are menadione, GSH and thiodione.

Instrumentation

This research uses software Gaussian 09 (Rev. D.01), AutoDock Vina (v1.2.3), Chemcraft (v1.8), PyMOL (v2.5.3), Avogadro (v1.2), ORCA (v5.0.0), VMD (v1.9.4), DFTB+ / DCDFTB (v23), LigPlot+ (v2.2), Discovery Studio (2022), dan Chimera (v1.16). The software is used for geometry optimization and energy calculations of protein compound structures. Autodock Vina was used for molecular docking calculations and chimera was used to create DCDFTB input files. For the calculation of the structural energy of the AIF and menadion, GSH and thiodion protein complexes, Orca software was used to optimize the geometry. In addition, Pymol, Ligplot, and Avogadro software were used to visualize the docking results and visualize the protein structures of AIF, AIF(FAD), AIF(NADH), and AIF(FAD)/(NADH) ligand ligands.

Procedures

Three-dimensional crystal structure of Apoptosis Inducing Factor (AIF) protein with code (Mate, 2022). The following PDB 3GD4 in complex with its ligands was taken from the Protein Data Bank (http://www.rscb.org/pdb) (Sevrioukova, 2009). The mediator used in this research; oxidized flavin adenine dinucleotide (FAD), nicotinamide adenine dinucleotide (NADH), 2methyl-1,4-naphthaquinone (menadione), reduced glutathione (C10H17N3O6S, GSH), menadion-S-SG (thiodion) were obtained from PubChem data(http:/ /pubchem.ncbi.nlm.nih.gov/).

Docking of the AIF receptor with menadione, GSH, and thiodion ligands was carried out. Autodock Vina is the program used for this computation, and all input files are set up in.pdb and.pdbqt formats. At this point, an AIF protein input file with the code 3DG4 downloaded from the protein Data Bank is being used. Re-docking was done initially, then docking

calculations with the menadion, GSH, and thiodion ligands. Making ensuring that the ligand's location aligns with the protein's active site is the goal. The native ligand, which serves as the native ligand, is docked out of PTP and then docked back into PTP to perform redocking. The test ligands were docked to get binding energy data in kcal.mol-1 units. The more negative the binding energy value, the greater the possibility of interaction leading to the formation of bonds.

The next calculation is to use DCDFTBMD for more detailed calculations of receptor and ligand interactions resulting in the best binding energy values for quantum docking of molecules in massively large systems with parallel computers (Nishimura & Nakai, 2019). In order to identify the involved residues, PMV is used to display protein ligand energy data. The data on interacting amino acids and interaction energy levels are the outputs of the docking computations.

RESULTS AND DISCUSSION

Ligan-AIF Molecular Docking

The geometric structures of the ligands that play a role in AIF were obtained, namely FAD, NAD, Menadion, GSH and Tiodion which had been optimized, and the AIF protein whose structure had been repaired using a modeler and then minimized using NAMD. AIF receptors that have been minimized using NAMD software have a structure that is more flexible, not rigid, like the initial structure which is still a crystal. Ligand-receptor interactions in the crystal structure are used as a reference, such as the number of residue contacts, the type of residue contacts, the number of hydrogen bonds, and the Root Mean Standard Deviation (RMSD). This information is taken from PDB. All parameters were compared by docking experiments of each receptor-ligand interaction. When the experiment has high similarity to the reference and the RMSD value is <2, the experimental system will be approved. The results showed that the docking program setup used in this experiment was quite good at predicting receptor-ligand interactions. (**Table 1**).

The results of the energy affinity between AIF protein and native PDB FAD ligand pose 1 show lower results -11.4, then thiodione ligand pose 1 with the lowest energy affinity -8.5, menadione pose 1 with the lowest energy affinity -7.0 and GSH ligand pose 1 with the lowest energy affinity -6 ,9. The following docking results show an analysis of a quinone compound, menadione, and show that in addition to reducing menadione, AIF is also involved in arylation with the antioxidant glutathione (GSH) by forming a thiodione compound, as shown by the lower and more stable affinity energy of the thiodione compound. Enzymatic reduction systems also had an impact on the cytotoxic level of quinones in the research of functional group interactions between menadione and AIF.

Differences in binding affinity between ligands are influenced by several molecular factors. Ligands such as FAD exhibit the strongest binding to AIF, likely due to their larger and more rigid structures that allow extensive interactions—such as hydrogen bonding and π-π stacking—with the protein binding site. Thiodine also exhibits relatively strong binding, likely due to favorable shape complementarity and chemical compatibility with the binding pocket. In contrast, ligands such as GSH and Menadione exhibit weaker affinities, likely due to their smaller size, greater flexibility, and fewer functional groups available for strong interactions. In addition, the loss of conformational entropy during binding and the mismatch between the ligand surface properties and the protein environment may further reduce their binding efficiency.

After validating, docking experiments were applied to menadione upon binding with AIF. This process reveals the energy affinity value, as a parameter of the bond strength between the ligand and the receptor. Lower energy affinity values indicate better binding stability. The binding energy is usually supported by interactions between the functional groups of the ligands to contact the enzyme residues. The information on interacting amino acids and interaction energy levels come from the docking calculations. This calculation's output is the input file that will be used during the DCDFTBMD step.

Table 1. Docking Binding Affinity

Complex (Protein+Ligan)							
Docking Minimization							
AIF-FAD		AIF-Menadion		AIF-GSH		AIF-Tiodion	
-11.4	**0.000**	**-7.0**	**0.000**	**-6.9**	**0.000**	**-8.5**	**0.000**
-9.7	2.704	-7.0	2.799	-6.8	3.435	-7.7	1.325
-9.7	3.741	-7.0	2.748	-6.6	12.345	-7.2	2.547
-8.7	8.900	-7.0	2.585	-6.5	1.794	-6.9	3.634
-8.6	8.721	-6.9	2.838	-6.5	7.655	-6.9	3.338
-8.5	8.863	-6.9	3.003	-6.5	2.095	-6.5	2.735
	-	-6.5	1.047	-6.3	12.297	-6.4	14.669
	-	-6.3	2.109	-6.3	2.753	-6.4	1.941
	-	-6.3	2.783	-6.2	7.930	-6.3	14.676

Analysis of Menadione and GSH Binding Affinity

Further investigations mentioned above that the arylation capacity of menadione involving protein thiols, computational studies were applied to determine the affinity of arylation precursors; menadione and GSH to AIF. Given the AIF cytotoxicity menadione modulation and during that time AIF is in the mitochondria (associated with the N-terminal domain) [trott]. Computational approaches focus on the FAD domain of AIF).ns were undertaken to investigate the role of other AIFs to modulate menadion arylation.

Docking visualizations of AIF with FAD, Menadione, and GSH show distinct binding interactions and ligand orientations. In the FAD complex (**Figure 1a**), the ligand is located deep within the binding pocket, forming strong interactions with key residues—colored blue for positive charges, red for negative charges, green for polar, and yellow for hydrophobic residues—indicating a stable and highly favorable binding. Menadione (**Figure 1b**) binds more superficially, primarily through hydrophobic contacts, while GSH (**Figure 1c**) exhibits a flexible, surface-based binding posture with fewer interactions. Menadione interacts with the AIF-menadione receptor residue ser175, which binds hydrogen bonds with an interaction distance of 3.32 A, at the best energy in pose 1. This corresponds to the contact residue on PDB AIF-FAD on the contact residue ser175, which binds hydrogen bonds 3.15 and the N-O bond with an interaction distance of 3.21 A. Interaction analysis showed this interaction. Although menadione is retained by the same number of contact residues and not much in each binding, the suitable binding environment for menadione is AIF. AIF-thiodion has more polar contact residues than AIF-menadione, which corresponds to the polarity of menadione.

Analysis of Thiodione Binding Affinity

Further investigation is used to understand the interaction model between AIF and thiodion. The results showed that thiodion had a better affinity for AIF than menadione or GSH. The energy affinity showed -7.0kcal/mol in the AIF-menadion (or AIF-GSH) interaction, compared to -8.5 kcal/mol in the AIF-thiodion interaction (**Table 1**). The interaction analysis showed that the AIF-thiodione receptor residues Ser175 (hydrogen bonded with a distance of 3.19), Arg284 (N-O bonds with a distance of 3.17), Asp437 (N-O bonds with a distance of 3.03), and Thr140 (bond distance of 3.03) interact with thiodion at the best energy at pose 1. The contact residue in PDB AIF-FAD at the contact residue ser175 which is bound to hydrogen bonds O-O spacing of 3.15 Å and the N-O bond with interaction spacing of 3.21 Å matches to His454's O-O bond spacing of 3.19 Å and the O-O spacing of 3.06 Å. Interaction analysis showed that thiodion was recognized by AIF residues more than menadione or GSH by AIF residues (**Figure 4**). This shows that the binding of AIF-thiodion is more stable compared to AIF-menadione or AIF-GSH.

Rescoring Ligand-AIF Interaction Using DCDFTBMD

In order to gain a deeper interaction for understanding the function of AIF, the interaction results obtained from the docking results are now calculated utilizing the DCDFTB approach at the quantum level. Calculations in this method in the first stage are DCDFTB calculations without prior optimization. From the calculation results, the binding energy data for each interaction is shown in (**Table 2**). The calculated energy data shows that there is a best energy difference in the results of docking with the DCDFTB method, that the best energy is not in the first pose but in a different pose for each interaction. This shows that the quantum calculation method can provide more detailed calculation data because the calculations carried out are up to the calculation of each atom.

The DCDFTB AIF-FAD interaction analysis at the best energy at pose 2 interacts with 11 receptor residues and has five residues that agree with the PDB data: Arg171 with N-O bonds and a bond distance of 2.74A, Arg284 with N-O bonds and a bond distance of 2.90A, Ala141 with an N-O bond and a bond distance of 3.08A, ASP437 with an N-O bond and a bond distance of 2. From the binding energy data of the AIF-FAD1 complex, the docking results show that the best affinity energy is at pose 1, while the best affinity energy calculated by DCDFTBMD is at pose 2. The difference can be seen in the interaction at serine 175 residue (**Figure 3**).

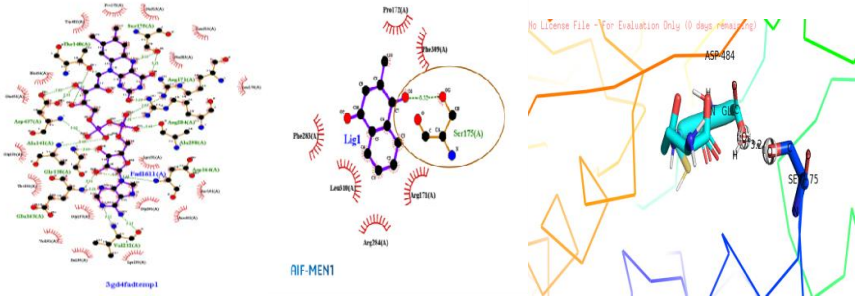

Figure 1. Visualization of docking results of AIF with FAD (**a**) PDB crystal structure and the results of AIF docking residues with menadione (**b**), and GSH (**c**) ligands.

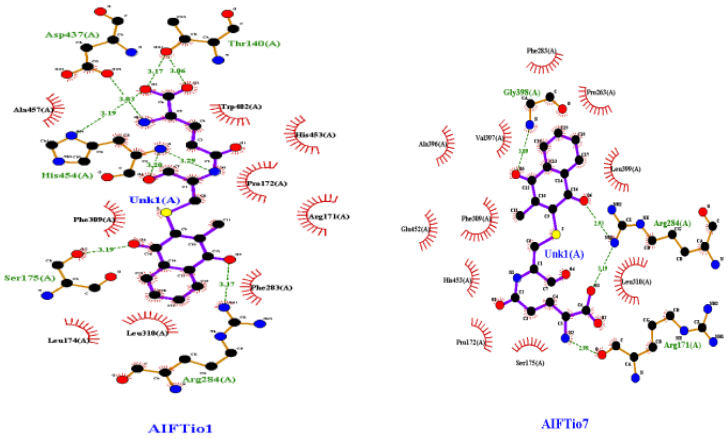

Figure 2. Visualization of the best results of docking residues AIF-thiodion pose 1, and AIF-thiodion pose 7 least amount of bound residue.

Table 2. Energy data for DCDFTB calculations on AIF receptor binding and FAD, Menadion, GSH and thiodion ligands.

Rescoring minimization			
AIF-FAD	AIF-Menadion	AIF-GSH	AIF-Tiodion
-1406.12	-1080.60	-1121.02	-1164.31
-1534.31	-1077.98	-1113.97	-1107.60
-1397.74	-1077.47	-1118.62	-1122.04
-1366.86	-1099.51	-1133.25	-1179.25
-1413.12	-1102.46	-1123.77	-1126.93
-1375.94	-1120.72	-1098.01	-1094.27
-1333.03	-1109.11	-1064.75	-1080.51
	-1123.98	-1096.62	-1106.10
	-1105.87	-1121.75	-1096.49

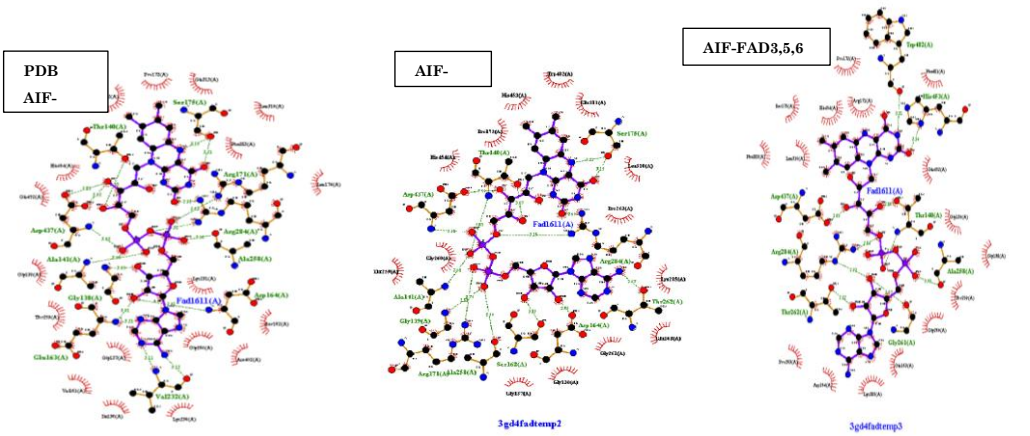

Figure 3. Visualization of the best energy interaction

In pose 1 the oxygen atom of the serine bonds with the hydrogen of the ligand at a distance of 3.21 Å while in pose 2 the serine 175 bonds with the hydrogen of the ligand with a distance of 3.15. This shows that in pose 2 the hydrogen interaction is stronger.

The oxygen charge on the FAD pose 1 ligand before the complex was 0.0816 while after the AIF-FAD1 complex was -0.5568. In pose 2 the oxygen charge on the menadione ligand before the simulation was 0.1363 while after the simulation it was -0.1879. This shows that the calculation results obtained a more negative charge value. This means that a stronger interaction is obtained because it is more electronegative, this indicates that there is a stronger attracting force for other electrons due to a polarization effect, this indicates that there is a transfer of electrons from AIF to FAD (**Figure 4**).

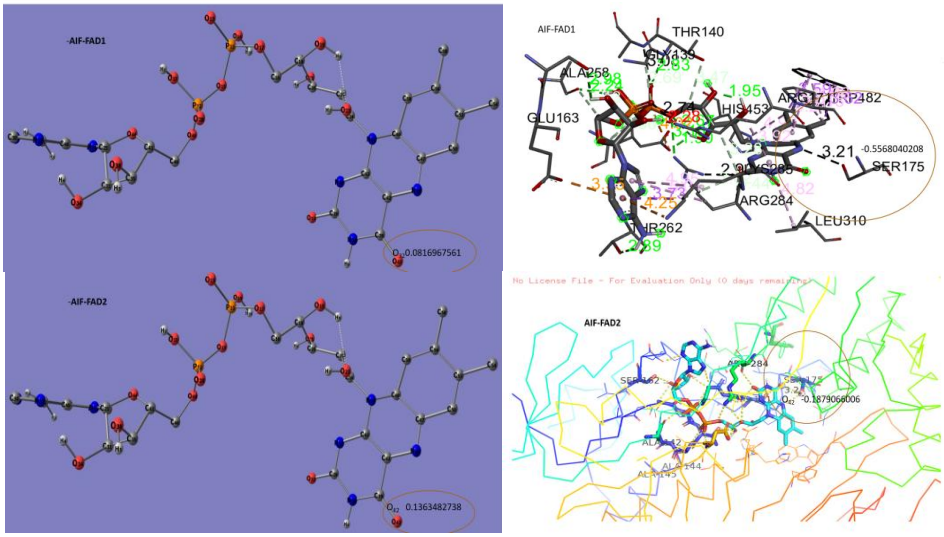

Figure 4. Residue contact, bond distance and charge of -FAD1

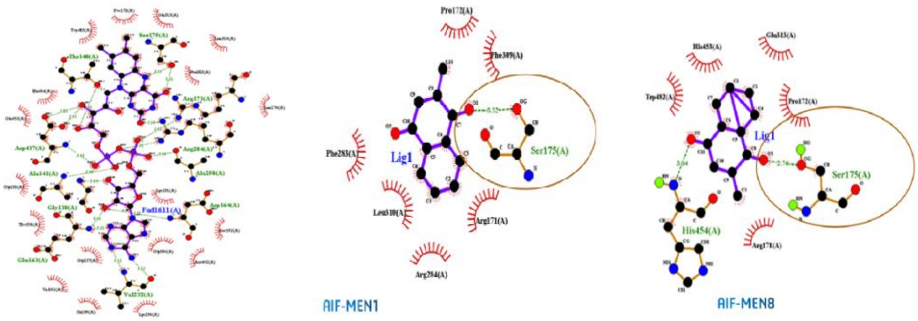

Figure 5. The visualization results of docking of 1 AIF-Men1(**a**) hydrogen bond and 2 AIF-Men8(**b**)

The following research was done on menadione ligands as quinone compounds that are involved in the control of AIF interaction. At the best energy in pose 8, the DCDFTB AIF–menadione interaction analysis shows interactions with two receptor residues and identifies two residues that match the PDB data. These two residues are His454, with an N–O bond and a bond distance of 3.04 Å, and Ser175, with an O–O bond that corresponds to the contact residues in PDB AIF–FAD. The O–O bond interaction distance at pose 8 for Ser175 is 2.74 Å, which is closer than the O–O bond distance at pose 1 for Ser175, which is 3.32 Å. This proves that the hydrogen bond interaction at pose 8 is stronger compared to pose 1. This data shows that the pose, based on the DCDFTB calculation, indicates that pose 2 is bound to more contact residues compared to the contact residues obtained in pose 1 (**Figure 5**).

In addition to residues and payload distances in the DCDFTB calculation, payload data is also obtained. The oxygen charge on the menadione pose 1 ligand before the complex with DCDFTBMD calculations is −0.3140, while after the AIF-Men8 complex, it is 0.3090. At pose 8, the oxygen charge on the menadione ligand before the complex is −0.3140, while after the AIF-Men8 complex, it is −0.3579 (Figure 6). This shows that the calculation results yielded a more negative charge value. This means that a stronger interaction is obtained because it is more electronegative. This indicates that there is a stronger attracting force for other electrons due to a polarization effect. This indicates that there is a transfer of electrons from AIF to menadione.

The following research was also done on GSH ligands as thiodion molecules that were produced experimentally when antioxidant arylation (GSH) interacted with menadion in AIF interactions. Analysis of DCDFTB interactions AIF-thiodion at the best energy at pose 4 interacts with 2 residues from the receptor and has 2 residues in agreement with the PDB data, namely his454 with an N-O bond and a bond distance of 2.87 Å, and a residue ser175 with an O-O bond of 3.19 Å, arg284 with an N-N bond and a bond spacing of 3.39 Å and phe309 with an N-O bond a bond spacing of 3.39 Å corresponds to the contact residue in PDB AIF-FAD.

Before the DCDFTBMD simulation, the oxygen charge on the menadion posture 1 ligand was -0.5019, and after the simulation, it was -0.4995. The oxygen charge on the menadione ligand at posture 8 was -0.4781 before the simulation and -0.4916 after. This demonstrates that a larger positive charge value was acquired from the simulation findings for the AIF-Tio interaction. Because it is more electropositive, this indicates that there is a stronger ability to take other electrons, which results in a stronger contact.

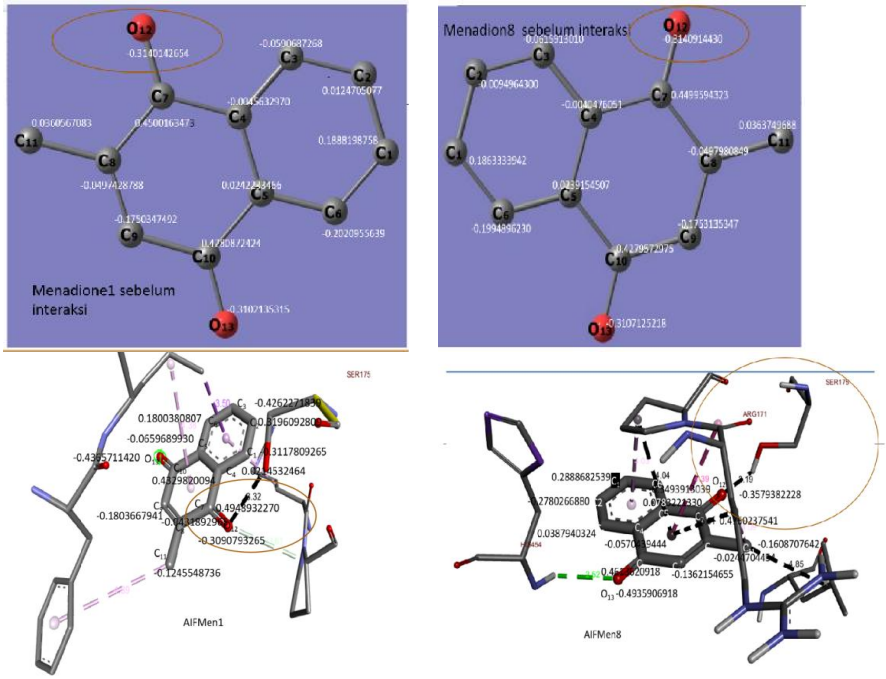

Figure 6. Menadion(**a**,**b**) Ligand Residue Contact Before and After Complexation with AIF-Men1(**c**) and AIF-Men8(**d**)

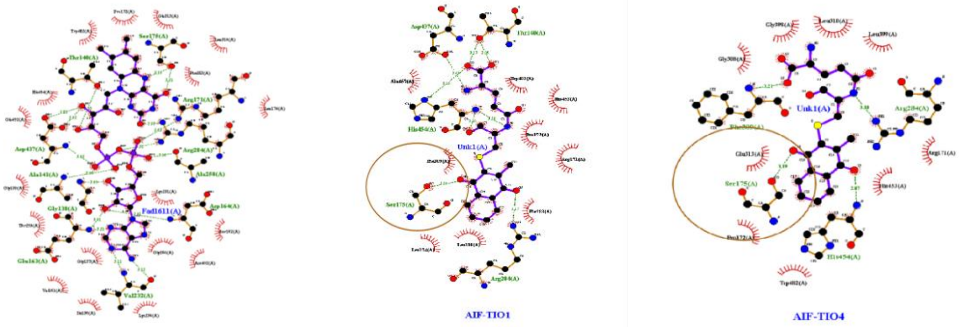

Figure 7. The two best postures of vina docking where one AIF-thiodion1 hydrogen bond and two AIF-thiodion4(**b**) hydrogen bonds are formed.

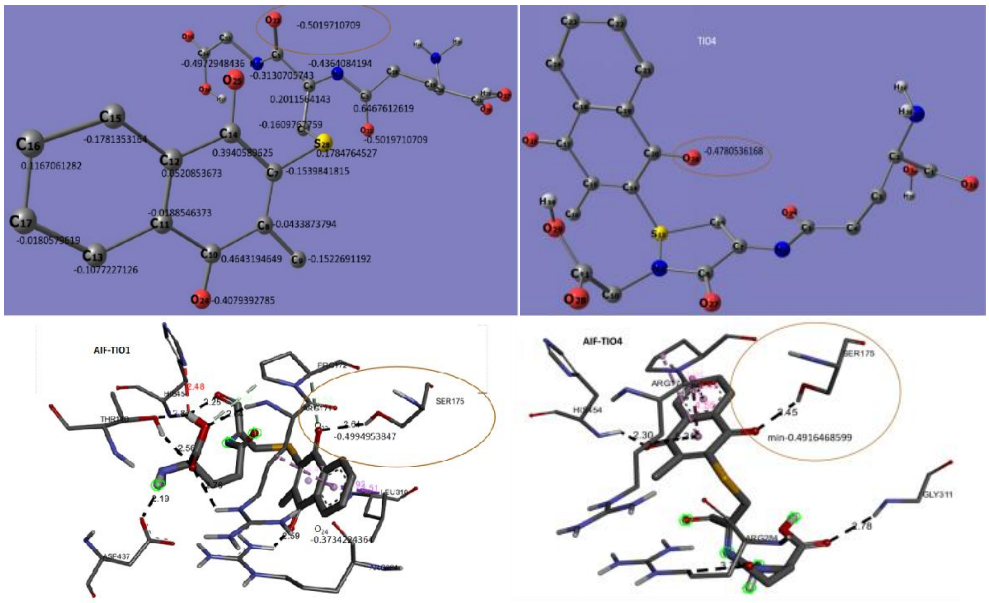

Figure 8. shows the contact between ligand residues in the thiodion(**a**,**b**) before and after the combination with AIF-Men1(**a**).

Parametrized Quantum Optimization on AIF Complexes

At this point, rescoring computations are performed so that the system is made dynamically active through optimization. **Table 3** displays the computed energy value of each ligand and complex together with the combined energy of each. The lowest binding energy was determined at the interactions of AIF-FAD pose 2, AIF-Menadione pose 8, AIF-GSH pose 9, and AIF-thiodion pose 9 based on the results of energy data calculations using DCDFTBMD with opt. This illustrates how the dcdftb method without opt and dcdftb with opt obtained data on binding energy values at the best possible different poses for each receptor and ligand. However, the binding energy data indicates the lowest energy at the same pose for the AIF-FAD and AIF-Menadion receptors. When the calculation system in the DCDFTB calculation method with opt is made dynamic, the interactions that take place become more dynamic and the energy changes.

Analysis of the interaction by DCDFTB AIF-thiodion at the best energy at pose 9 interacts with four receptor residues and has three residues that agree with the PDB data, namely residue his454 with N-O bonds and a bond distance of 2.87A, residue ser175 with O-O bonds and a bond distance of 3.19A, and residue arg284 with N-N bonds and a bond distance of 3.39A. This information demonstrates that pose 9, which is based on the DCDFTB calculation, is bound to the same contact residue to a greater extent than pose 1, which corresponds to the PDB data, and that pose 9 and pose 1 share the same O-O bond interaction distance at ser175, which is 3.36A. Ser175 and His454 are the two residues that bind with the receptor according to DCDFTB AIF-menadion's analysis of the interaction at the optimum energy at position 8.

According to **Figure 4a**, the menadione ligand's oxygen atom and the hydrogen atom in the serine175 residue form a hydrogen bond with an interaction distance of 3.6 A, and the oxygen ligand's charge after complex is -0.3579. In **figure 4b**, the charge on the ligand after the complex is -0.4254, and the hydrogen bond distance between the oxygen on the GSH ligand and the oxygen atom on the serine175 residue has an interaction distance of 2.9A. With an interaction distance of 2.5A and a charge of -0.4916, the oxygen atom in the thiodion ligand and the hydrogen atom in the serine oxygen residue form a hydrogen bond in **Figure 4c**. Thiodion is the closest bond formed and has the highest negative charge among the three interactions, relative to menadion and GSH.

Table 3. Energy data for DCDFTBMD calculations on AIF receptor binding and FAD, Menadion, GSH and thiodion ligands.

Total Energy of Minimization Rescoring (E_Bind= E_kompleks-E_protein-E_ligan) kkal/mol			
AIF-FAD	AIF-Menadion	AIF-GSH	AIF-Tiodion
-3304.17	-3567.31	-3765.29	-3520.28
-3369.72	-3541.48	-3625.08	-3538.03
-3334.12	-3541.48	-3755.13	-3563.78
-3302.23	-3548.31	-3725.03	-3563.78
-3245.12	-3552.68	-3743.09	-3751.03
-3305.27	-3550.63	-3722.23	-3552.13
-3340.22	-3543,24	-3724.12	-3758.03
	-3554.78	-3722.25	-2289.96
	-2975.11	-3785.03	-3872.89

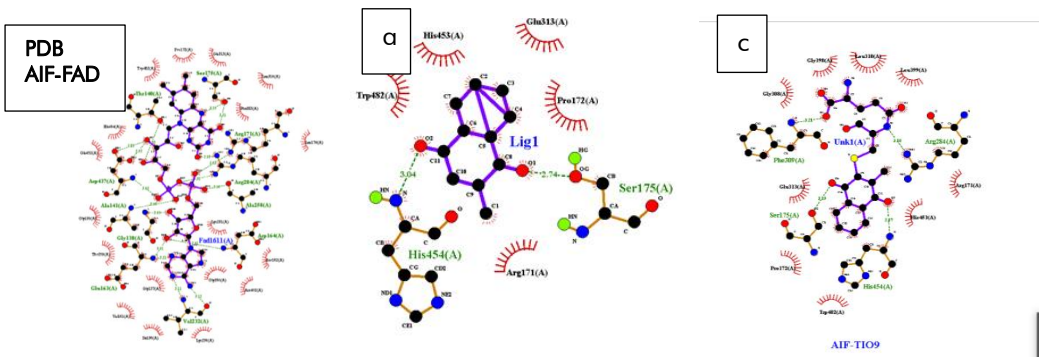

Figure 9. Visualization of the best poses for DCDFTBMD results with opt in to AIF-FAD PDB, AIF-Menadion pose 8(**a**), AIF-GSH pose 9, and AIF-Thiodion pose 9 (**c**) with hydrogen bonded residue data on ligands and receptor.

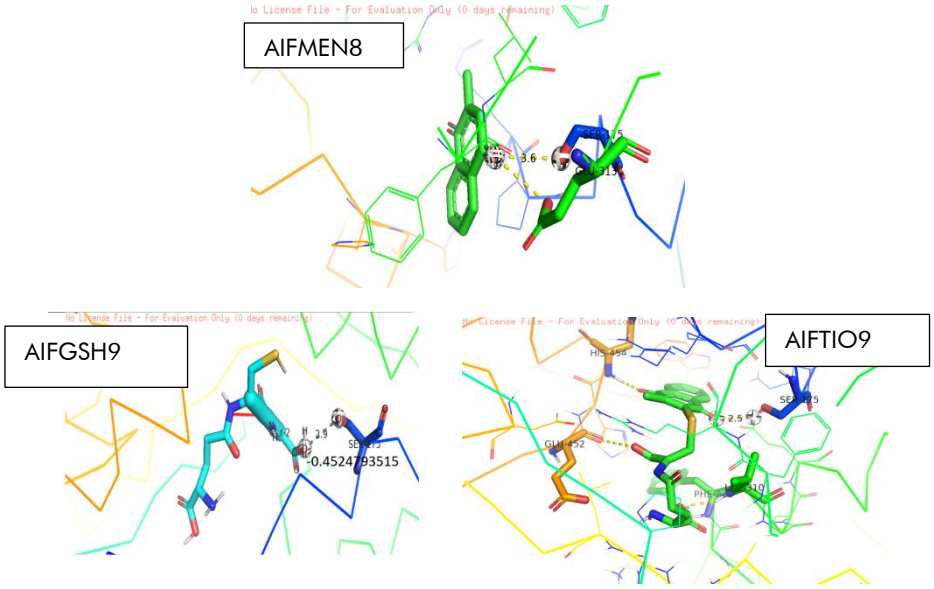

Figure 10. Remaining contact, interaction distance, and interaction charge from AIF-Menadion8, AIF-GSH9, and AIF-thiodion9 following complex's optimum energy poses.

This demonstrates the polarization of the AIF receptor and quinone ligand interaction. This demonstrates that calculations made with the DCDFTBMD technique can clarify in greater detail how the AIF-mitochondria regulate arylated quinone molecules with gluthation to generate more stable thiodion compounds, enhancing the function of AIF in the process of cell death. These results are consistent with previous studies showing that AIF, as an FAD-containing flavoprotein, interacts with quinone-based compounds through redox and electrostatic mechanisms. For example, studies by Miramar et al. (2001) and Milczarek et al. (2013) showed that AIF can form charge transfer complexes with quinones such as menadione, highlighting its affinity for redox-active ligands. Consistent with this, ligands such as FAD and thiodione—which have polar and electron-rich structures—showed stronger binding in our docking analysis, indicating their potential as lead compounds for drug development targeting AIF. These ligands exhibit greater charge polarization, increasing electrostatic complementarity, and stabilizing the AIF-ligand complex.

CONCLUSIONS

Based on DCDFTBMD quantum mechanical calculations, each ligand—FAD, menadione, GSH, and thiodion—interacts with the AIF receptor through distinct conformations, with optimal binding observed at different poses: pose 2 for FAD, pose 8 for menadione, and pose 9 for both GSH and thiodion. OPT-based DCDFTB calculations also confirmed this variation, highlighting key binding poses and the involvement of critical amino acid residues, particularly Ser175, a known interaction site for FAD and quinone-type ligands. These results suggest that binding to this conserved site may alter AIF function, potentially modulating its role in mitochondrial-induced cell death. The interaction patterns also suggest a polarizing effect between AIF and quinone ligands, contributing to binding stability and functional modulation. Key residues such as Ser175, His454, Arg284, Asp437, and Thr140 appear to play important roles in mediating ligand-specific interactions, particularly in the arylation of menadione. Collectively, these findings provide mechanistic insights into how AIF recognizes and binds quinone-based ligands, and support the potential of menadione as a promising anticancer agent through its ability to target and modulate AIF activity.

ACKNOWLEDGMENTS

KEMENAG-DIKTI scholarship research fund of doctoral program in 2016, continued independent funding. All authors are contributed equally and have read and agreed to the published version of the manuscript.

REFERENCES

Abad, Enrique., Zenn, K. R., & Kastner, J. (2013). Reaktion mechanism of monoamine oxidase from QM/MM calculations, *Journal Physical Chemistry, Computational Biochemstry Group, Institut of Theorical Chemistry, University of Stuttgart, Pfaffenwaldring, 55,* 70569

Acacio, S. d. S., Ruan. C. B. R., Dora. C. S. C., Fernanda. P. P., David. R. P., Matheus. G. d. M., Fernando. D. C. d. S., & Luana. D. S. M. (2022). Menadione: a plathform and a target to valuable compounds synthesis, *Beilstein Journal of Organic Chemistry, 18, 381–419*

Aditya, W,S., Yoshifumi, N., Hiromi, Nakai, J., (2017): Rigorous pKa Estimation of amine species using densityfunctional tight-binding-based

metadynamics simulations, *Journal of Chemical Theory and Computation, 14*(1), 351-356

Bano, D., & Prehn, J. H.M. (2018). Apoptosis-inducing factor (AIF) in physiology and disease: The tale of a repented natural born killer. *EbioMedicine, 30,* 29-37.

Cores, Á., Carmona-Zafra, N., Clerigué, J., Villacampa, M., & Menéndez, J. C. (2023). Quinones as neuroprotective agents. *Antioxidants, 12*(7), 1464

Fang, Y., & Peng, K. (2022). Regulation of innate immune responses by cell death-associated caspases during virus infection. *FEBS Journal, 289* (14), 4098–4111.

Galluzzi, L., Maiuri, M. C., Vitale, I., Zischka, H., Castedo, M., Zitvogel, L., & Kroemer, G. (2007). Cell death modalities: Classification and pathophysiological implications. *Cell Death & Differentiation, 14*(7), 1237–1243.

Kroemer, G., Galluzzi, L., Chatterinne, B., (2007). Mitochondrial membrane permeabilization in cell death. *Physiological Reviewes, 87*(I) : 99-163.

Lorenzo, H. K., Susin, S, A., Penninger, J.,Kroemer, G. (1999). Apoptosis Inducing Factor (AIF): a phylogenetically old, caspase-independent effector of cell death. *Cell Death and Differentiation, 6 516-524.*

Hangen, E., Blomggren, K., Benit, P., Kroemer, G. and Modjtahedi, N. (2010). Life with or without AIF. *Trends in Biochemical Sciences, 35, 5: 278-287.*

Jha, R.K and Kumar, S. (2024). Direct Functionalization of para-Quinones: A Historical Review and New Perspectives. *European Journal of Organic Chemistry, 27*

Mate, M. J., Ortiz-Lombardia, M., Boitel, B., Haouz, A., Tello, D., Susin, S, A., Penninger. J., Kroemer, G., Alzari, P.M. (2002). The crystal sructure of the mouse apoptosis-inducing factor AIF, Nature Structural Biology, 9, 6: 442-6Nakai, H., Sakti, A. W., & Nishimura, Y. (2016). Divide-and-Conquer-Type Density-Functional Tight-Binding Molecular Dynamics Simulations of Proton Diffusion in a Bulk Water System. *Journal of Physical Chemistry B, 120*(1), 217–221.

Milczarek, M., et al. (2013). AIF–menadione interaction promotes redox cycling and mitochondrial dysfunction. *Biochimica et Biophysica Acta (BBA) - Molecular Cell Research, 1833*(4), 711–722.

Miramar, M. D., et al. (2001). Apoptosis-inducing factor, a new flavoprotein involved in apoptosis and mitochondrial respiratory chain. *Journal of Biological Chemistry, 276*(1), 120–126.

Misevicience, L., Anusevicius, Z., Sarlauskas. J., Sevrioukova, I. F., Cenas, N. (2011). Redox reactions of the FAD-containing apoptosis-inducing factor (AIF) with quinoidal xenobiotics: a mechanistic study. *Archives of Biochemistry and Biophysics. 512*(2), 183-189.

Nishimura, Y., & Nakai, H. (2019). Dcdftbmd: Divide-and-conquer density functional tight-binding program for huge-system quantum mechanical molecular dynamics simulations. *Journal of Computational Chemistry, 40*(15), 1538–1549.

Sevrioukova, I. F. (2009). Redox-linked conformational dynamics in apoptosis-inducing factor. *Journal of Molecular Biology, 390* (5), 924–938.

Szeliga, M., & Rola, R. (2022). Menadione potentiates auranofin-induced glioblastoma cell death. *International Journal of Molecular Sciences, 23*(24), 15712

Vidal-Limon, A., Aguilar-Toalá, J. E., & Liceaga, A. M. (2022). Integration of molecular docking analysis and molecular dynamics simulations for studying food proteins and bioactive peptides. *Journal of Agricultural and Food Chemistry, 70*(4), 934–943.

Wiraswati, H. L., Hangen, E., Sanz, A. B., Lam, N. V., Reinhardt, C., Sauvat, A., Mogha, A., Ortiz, A., Kroemer, G., & Modjtahedi, N. (2016). Apoptosis inducing factor (AIF) mediates lethal redox stress induced by menadione. *Oncotarget, 7*(47), 76496–76507.

Software Citation

Avogadro: an open-source molecular builder and visualization tool. Version 1.XX. http:// avogadro.cc/

Biovia, D.S. (2019). *Discovery Studio Visualizer*. San Diego.

Chemcraft - graphical software for visualization of quantum chemistry computations. Version 1.8, build 682. https://www.chemcraftprog.com

Eberhardt, J., Santos-Martins, D., Tillack, A.F., & Forli, S. (2021). AutoDock Vina 1.2.0: New Docking Methods, Expanded Force Field, and Python Bindings. *Journal of Chemical Information and Modeling, 61*(8)

Gaussian 09, Revision A.02. (2016). M. J. Frisch, G. W. Trucks, H. B. Schlegel, G. E. Scuseria, M. A. Robb, J. R. Cheeseman, G. Scalmani, V. Barone, G. A. Petersson, H. Nakatsuji, X. Li, M. Caricato, A. Marenich, J. Bloino, B. G. Janesko, R. Gomperts, B. Mennucci, H. P. Hratchian, J. V. Ortiz, A. F. Izmaylov, J. L. Sonnenberg, D. Williams-Young, F. Ding, F. Lipparini, F. Egidi, J. Goings, B. Peng, A. Petrone, T. Henderson, D. Ranasinghe, V. G. Zakrzewski, J. Gao, N. Rega, G. Zheng, W. Liang, M. Hada, M. Ehara, K. Toyota, R. Fukuda, J. Hasegawa, M. Ishida, T. Nakajima, Y. Honda, O. Kitao, H. Nakai, T. Vreven, K. Throssell, J. A. Montgomery, Jr., J. E. Peralta, F. Ogliaro, M. Bearpark, J. J. Heyd, E. Brothers, K. N. Kudin, V. N. Staroverov, T. Keith, R. Kobayashi, J. Normand, K. Raghavachari, A.

Rendell, J. C. Burant, S. S. Iyengar, J. Tomasi, M. Cossi, J. M. Millam, M. Klene, C. Adamo, R. Cammi, J. W. Ochterski, R. L. Martin, K. Morokuma, O. Farkas, J. B. Foresman, and D. J. Fox (2016). *Gaussian, Inc., Wallingford CT*

Humphrey, W., Dalke, A. and Schulten, K. (1996). VMD - Visual Molecular Dynamics. *Journal of Molecular Graphics and Modelling,14,* 33-38.

LigPlot+: multiple ligand-protein interaction diagrams for drug discovery. *Journal of Chemical Information and Modeling, 51(*10): 2778-2786.

Marcus D Hanwell, Donald E Curtis, David C Lonie, Tim Vandermeersch, Eva Zurek & Geoffrey R Hutchison. (2012). Avogadro: An advanced semantic chemical editor, visualization, and analysis platform. *Journal of Cheminformatics, 4:17.*

Neese, F. (2012). *The ORCA program system*, Wiley Interdiscip.

Pettersen, E.F., Goddard, T.D., Huang, C.C., Couch, G.S., Greenblatt, D.M., Meng, E.C., and Ferrin, T.E. (2024) "UCSF chimera - a visualization system for exploratory research and analysis." *Journal of Computational Chemistry, 25*, 1605–1612

The PyMOL Molecular Graphics System, Version 3.0 Schrödinger, LLC

Trott, O. & A. J. Olson. (2010). AutoDock Vina: improving the speed and accuracy of docking with a new scoring function, efficient optimization and multithreading. *Journal of Computational Chemistry, 31(*2010) 455-461